Electronic Supplementary Material (ESI) for Physical Chemistry Chemical Physics.

Supporting Information

for

Mechanism of darunavir binding to monomeric HIV-1 protease: A step forward in rational design of dimerization inhibitors

Mohd Ahsan,[#] Chinmai Pindi,[#] and Sanjib Senapati*

Department of Biotechnology and BJM School of Biosciences,
Indian Institute of Technology Madras, Chennai 600036, India.
Ph:+91-44-22574122, e-mail: sanjibs@iitm.ac.in

[#] These authors contributed equally to this work.

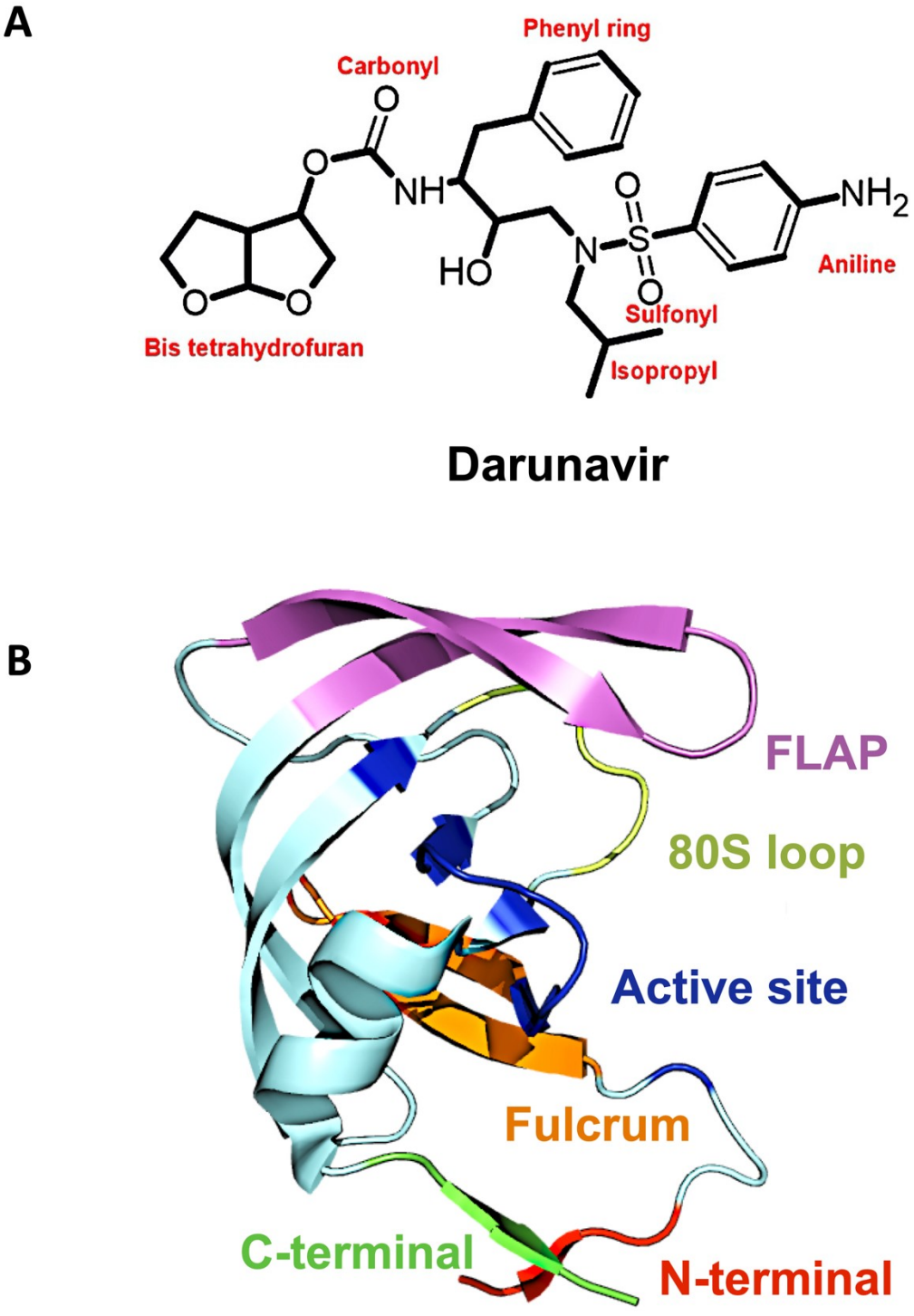

Figure S1: (A) Chemical structure of Darunavir. (B) 3D molecular structure of HIV protease monomer with important key regions highlighted.

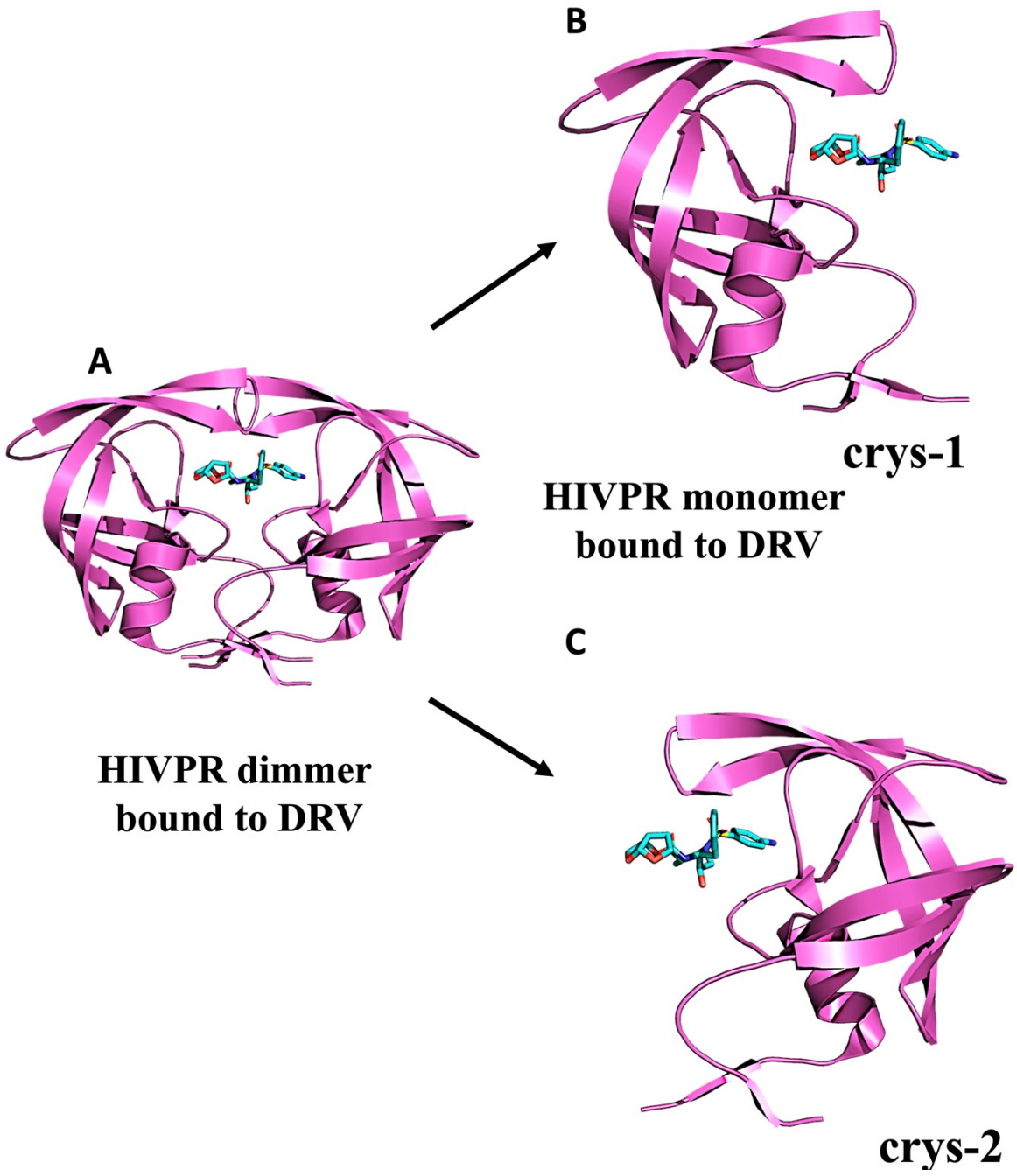

Figure S2: Starting DRV-mPR configurations from crystal structure. (A) Crystal structure of darunavir (DRV) bound wild type HIVPR dimer (PDB ID: 4LL3). Two starting structures of DRV bound monomeric HIVPR were created from this crystal structure as - (B) the monomer interacting with the furo(2,3-b)furan ring moiety of DRV is termed as crys-1, (C) the second monomer that interacts with the amino phenyl moiety of DRV is termed as crys-2.

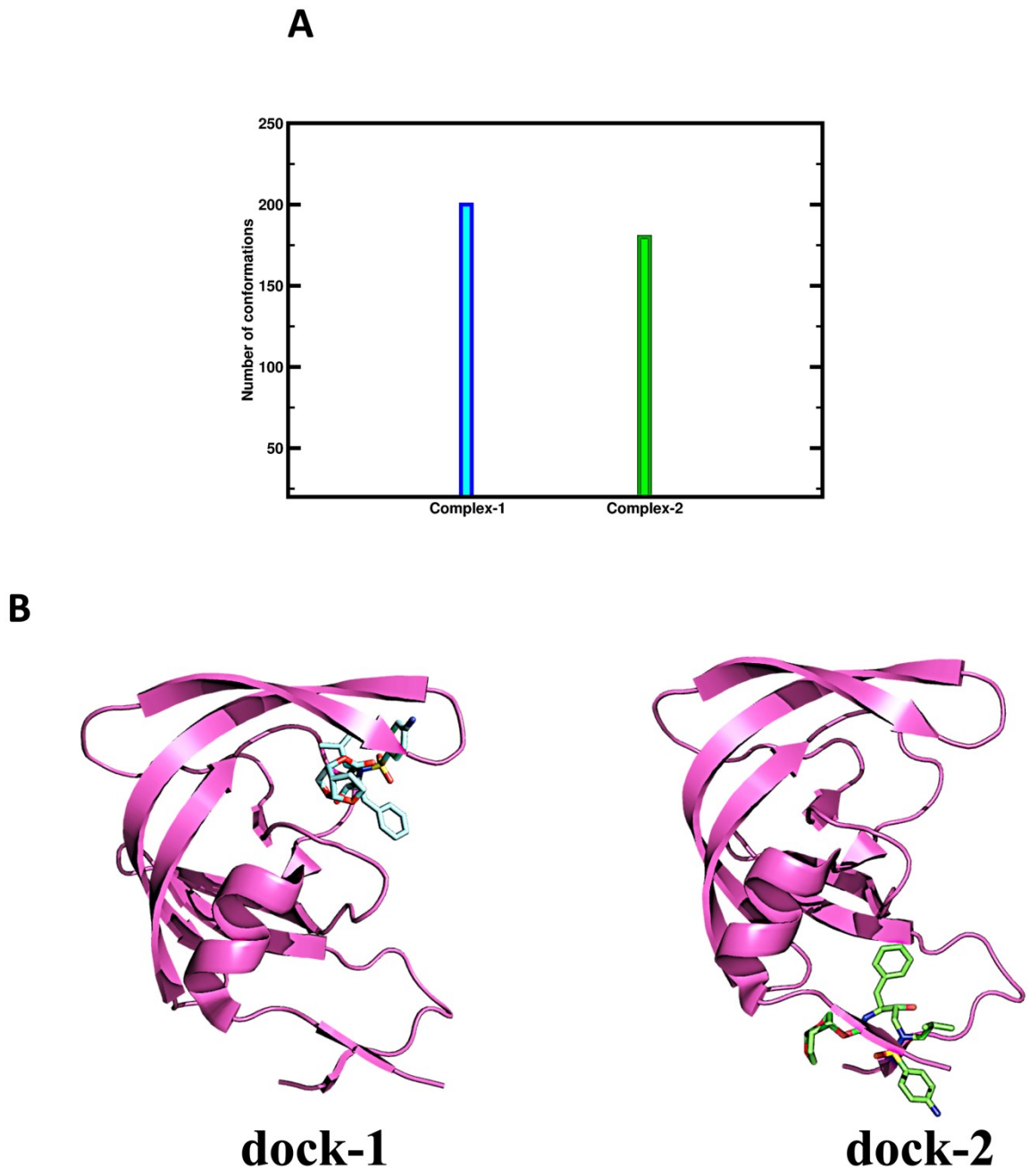

Figure S3: Starting DRV-mPR structures from protein-ligand docking studies. (A) Number of conformations in two major clusters from the docking study. The RMS tolerance used for clustering is 2 Å. (B) The binding pose of DRV to HIVPR monomer in the respective cluster. The complex in which DRV interact with flap is called dock-1 and the complex in which DRV interact with PR termini is called dock-2.

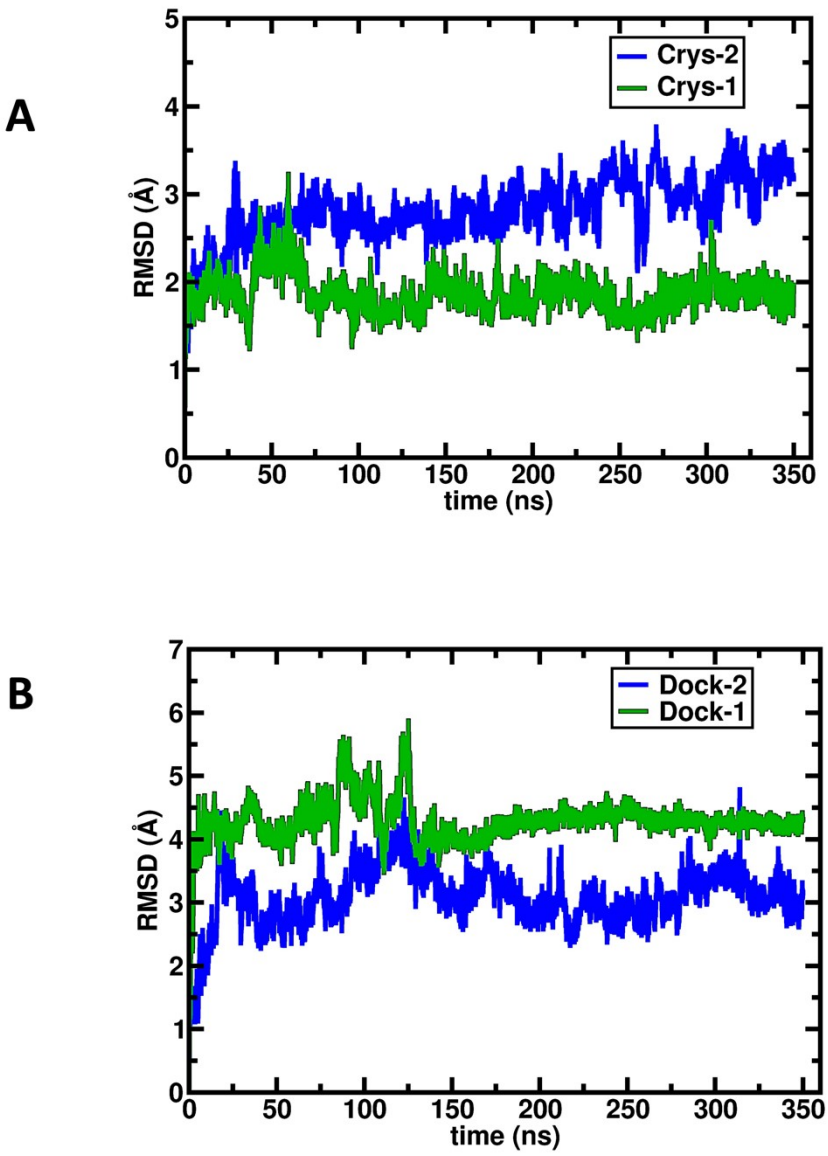

Figure S4: Time evolution of the protein RMSD in the structures created from the (A) DRV bound dimeric HIVPR X-ray structure and (B) blind docking of DRV to monomeric HIVPR (mPR). In both (A) and (B), two different initial binding poses of the ligand were examined as described in Figs. S2, S3.

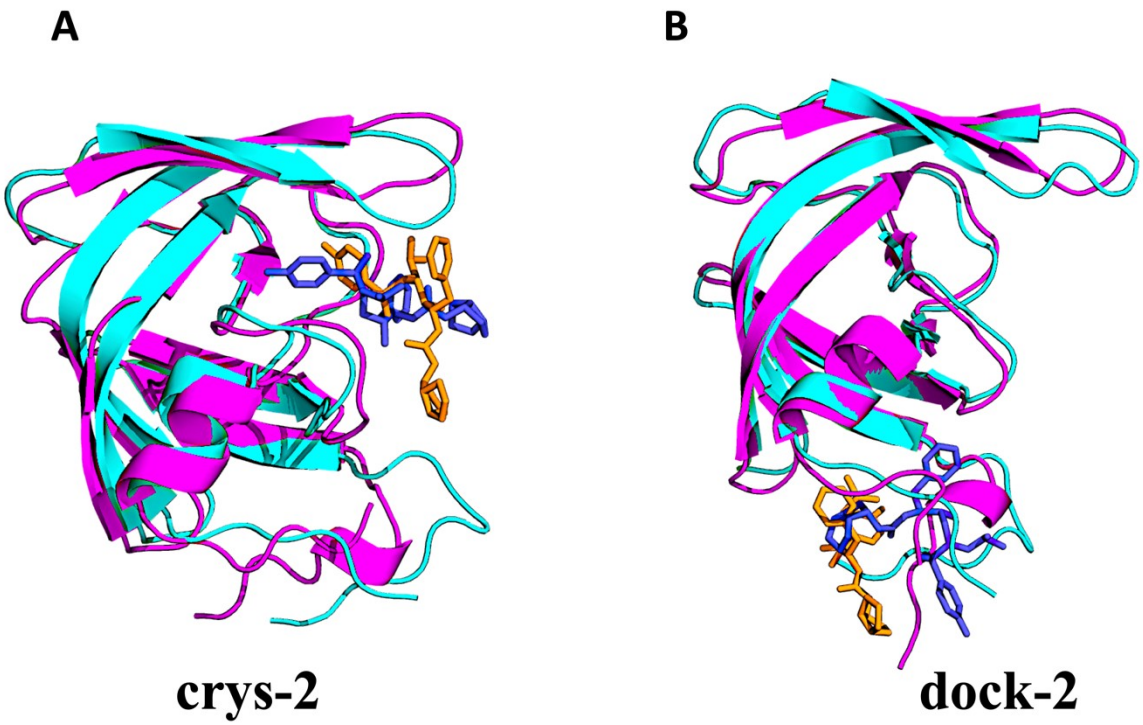

Figure S5: The 3D representations of the final binding pose of DRV to mPR are shown for the crys-2 and dock-2 complexes. These time-averaged final structures obtained from 350 ns independent MD simulations (protein: magenta, DRV: orange) are superposed over the respective starting conformation (protein: cyan, DRV: blue) to highlight the changes. The other two MD generated DRV-mPR complexes, crys-1 and dock-1 are shown in Fig. 1.

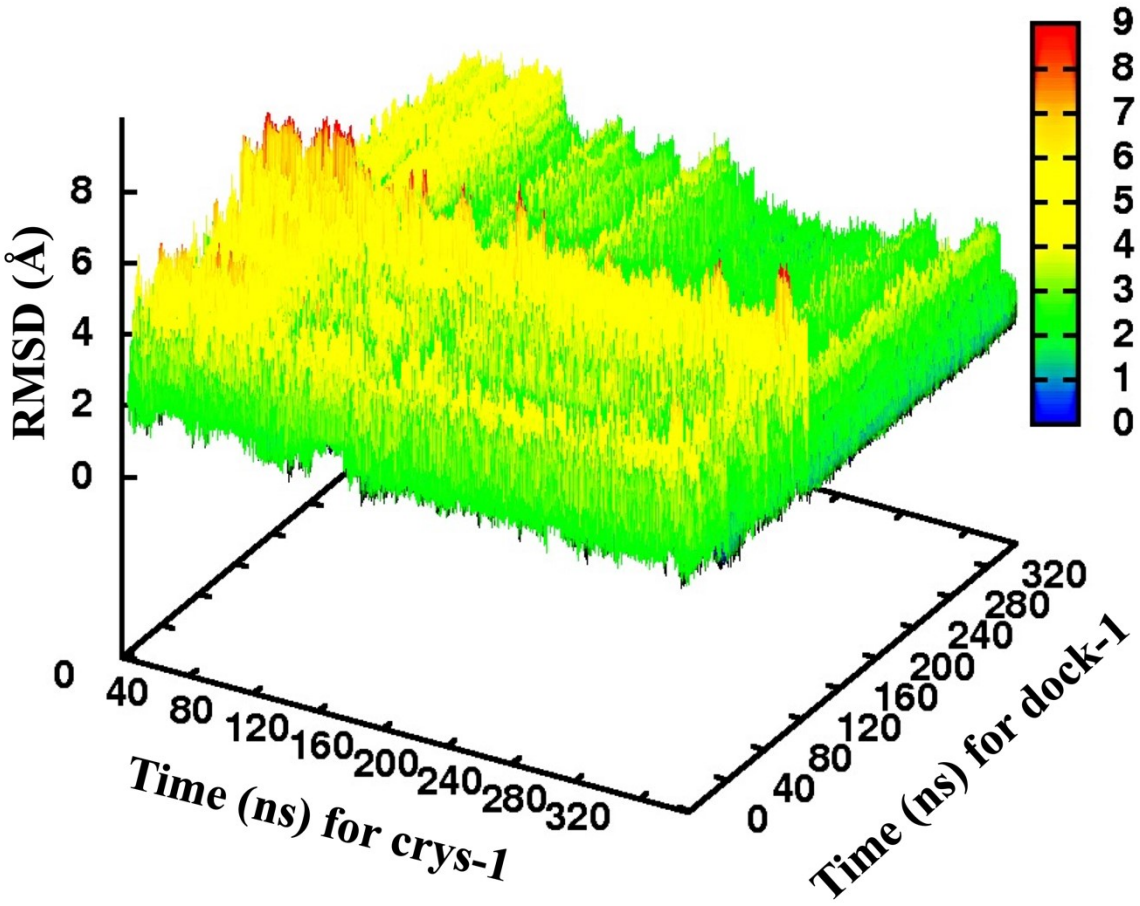

Figure S6: The 2D-RMSD profile of the protein backbone as generated by fitting the protein conformations obtained from the MD trajectories of the crys-1 and dock-1 complexes.

Table S1: Enthalpic and entropic contributions to the total binding free energy of DRV to protease monomers in crys-1 and dock-1. All energies are in kcal/mol.

System	ΔG_{Total}	ΔG_{MM}	ΔG_{Solv}	$T\Delta S$
Crys-1	-20.01 ± 3.7	-79.54 ± 8.6	32.26 ± 3.6	-27.26 ± 2.5
Dock-1	-23.12 ± 3.6	-89.94 ± 9.1	37.48 ± 3.5	-29.33 ± 2.8

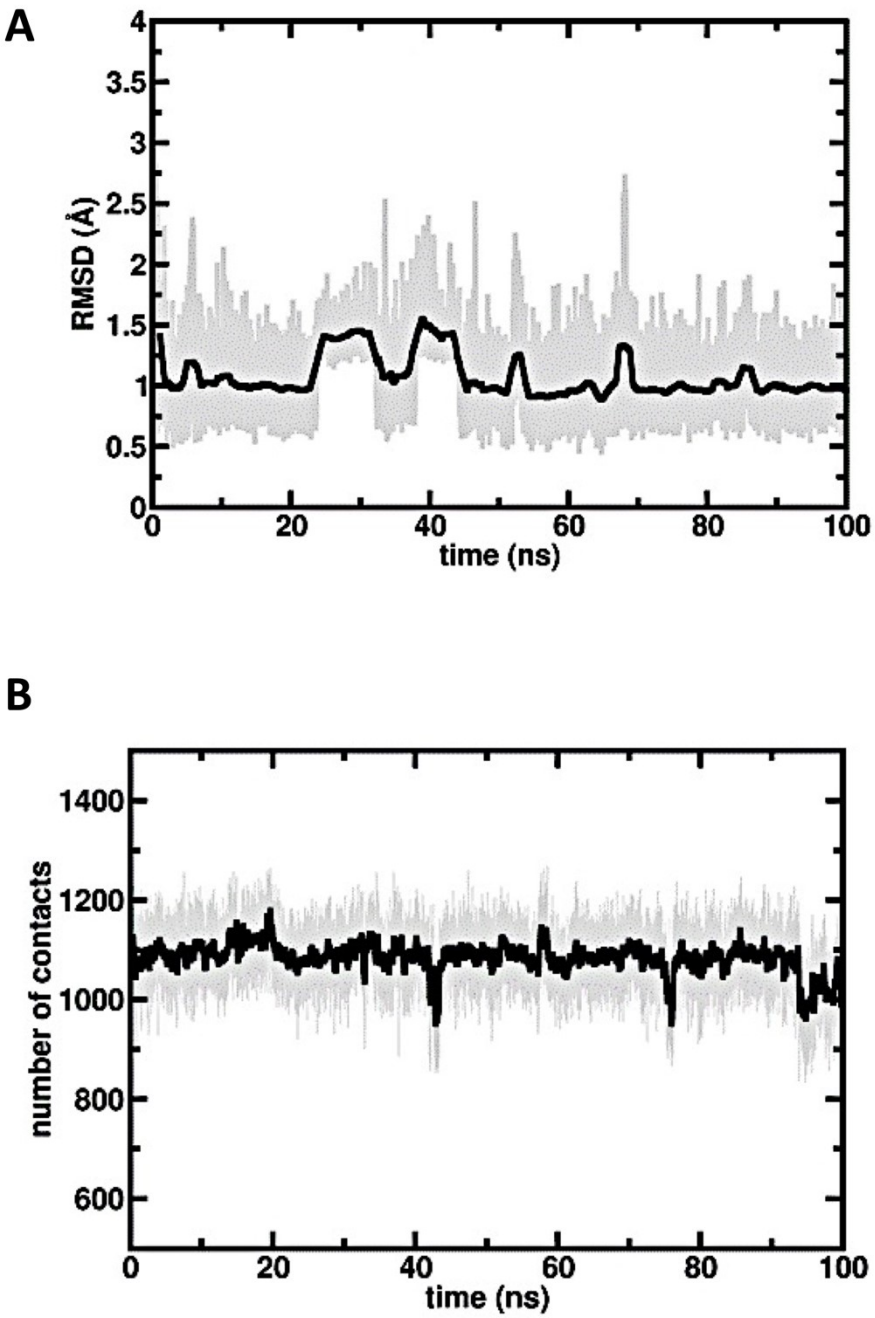

Figure S7: Formation of a stable DRV-mPR complex. Time evolution of the (A) ligand RMSD and (B) number of contacts between DRV and HIVPR monomer in the final structure.

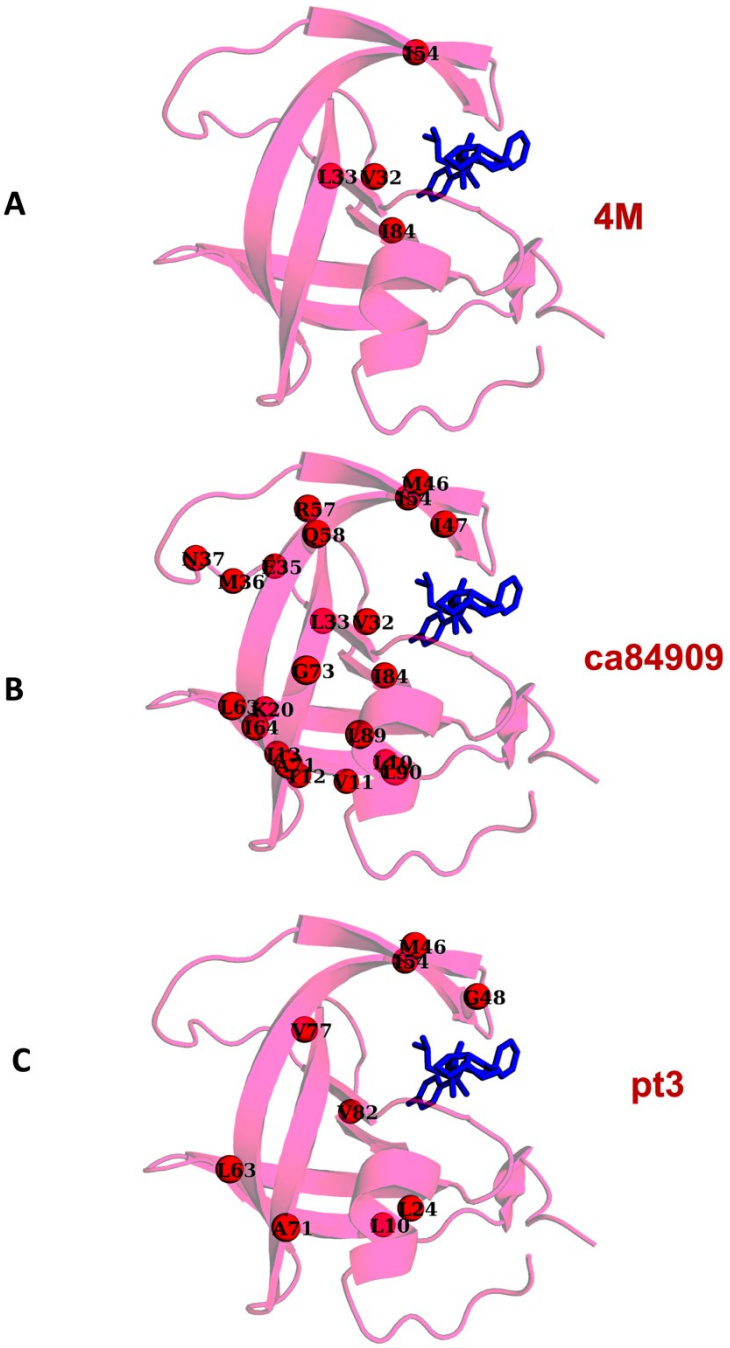

Figure S8: The locations of the mutated residues in the HIVPR variants - (A) 4M, (B) CA84909 and (C) pt3.

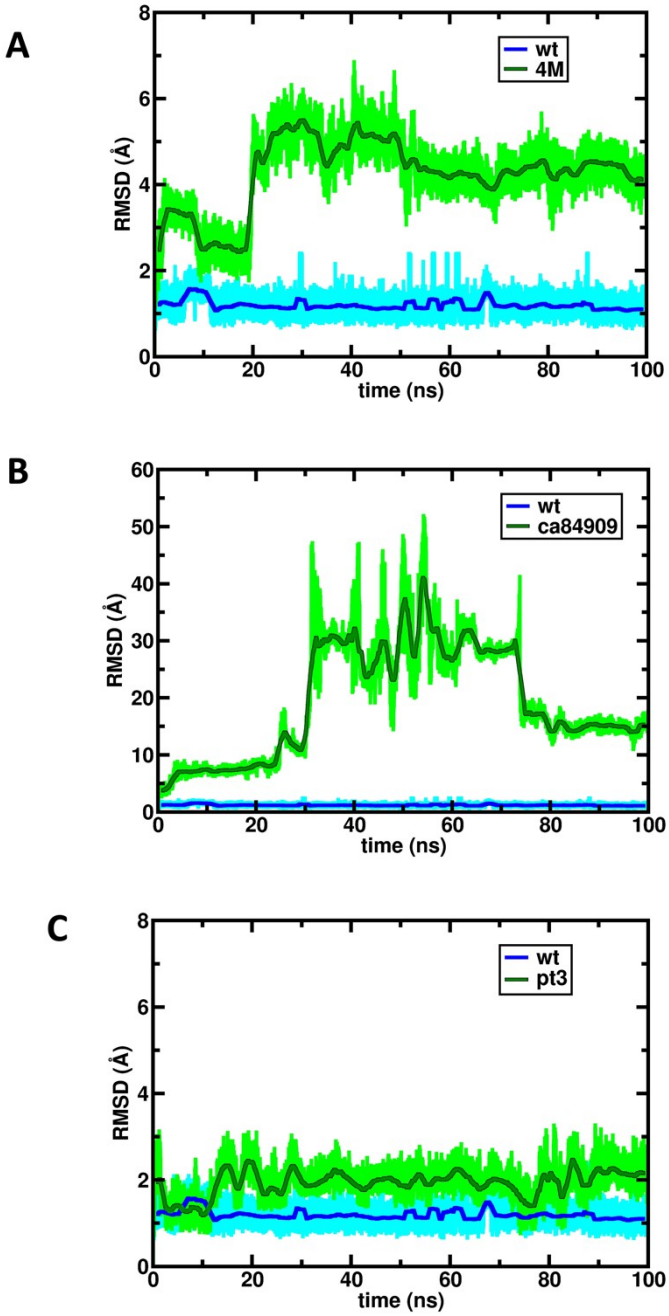

Figure S9: Time evolution of the ligand RMSD in the variant (A) 4M, (B) CA84909 and (C) pt3. For comparison, results are included for DRV bound to WT mPR.

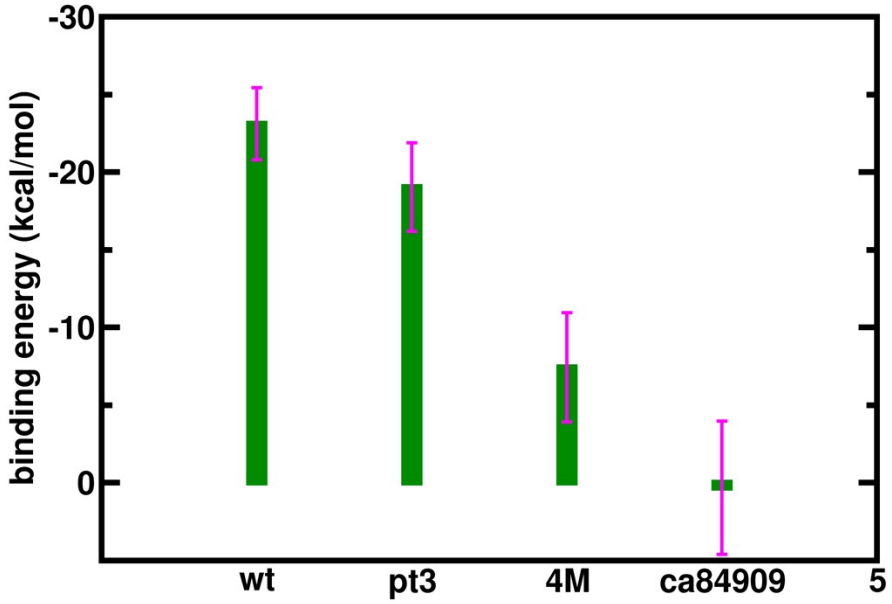

Figure S10: The binding free energy of DRV to HIVPR monomer in WT, pt3, 4M and ca84909 systems.

Table S2: Enthalpic and entropic contributions to the total binding free energy of DRV to protease monomers in pt3, 4M and ca84909 systems. All energies are in kcal/mol.

System	ΔG_{Total}	ΔG_{MM}	ΔG_{Solv}	$T\Delta S$
pt3	-19.04 ± 2.8	-87.59 ± 8.7	39.31 ± 3.4	-29.23 ± 3.5
4M	-7.44 ± 3.5	-63.29 ± 9.2	29.17 ± 3.8	-26.68 ± 3.7
ca84909	0.32 ± 4.2	-52.77 ± 9.8	26.67 ± 3.7	-26.41 ± 3.8

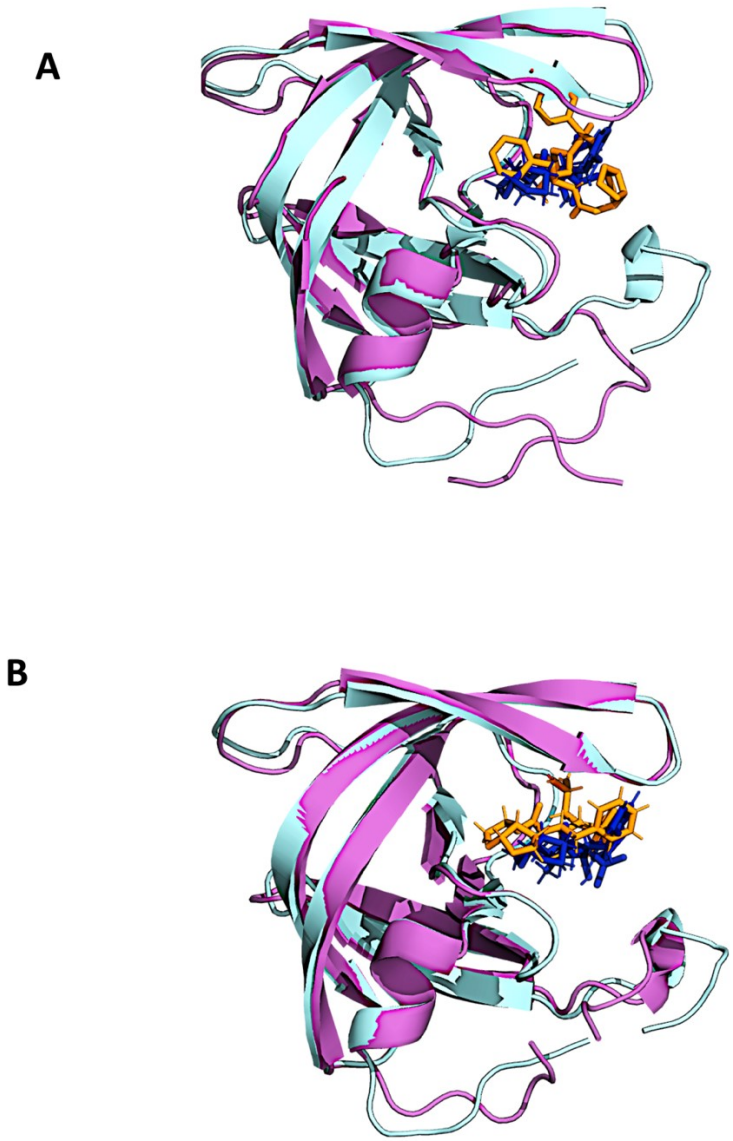

Figure S11: (A) Binding pose of DRV in the pt3 variant from blind docking (protein: magenta, DRV: orange). This structure was refined over 300 ns MD simulation and the obtained time-averaged structure is superposed (protein: cyan, DRV: blue). (B) Superposition of the time-averaged structure in (A) over the WT DRV-mPR complex. Color code: variant (protein: cyan, DRV: blue), WT (protein: magenta, DRV: orange).

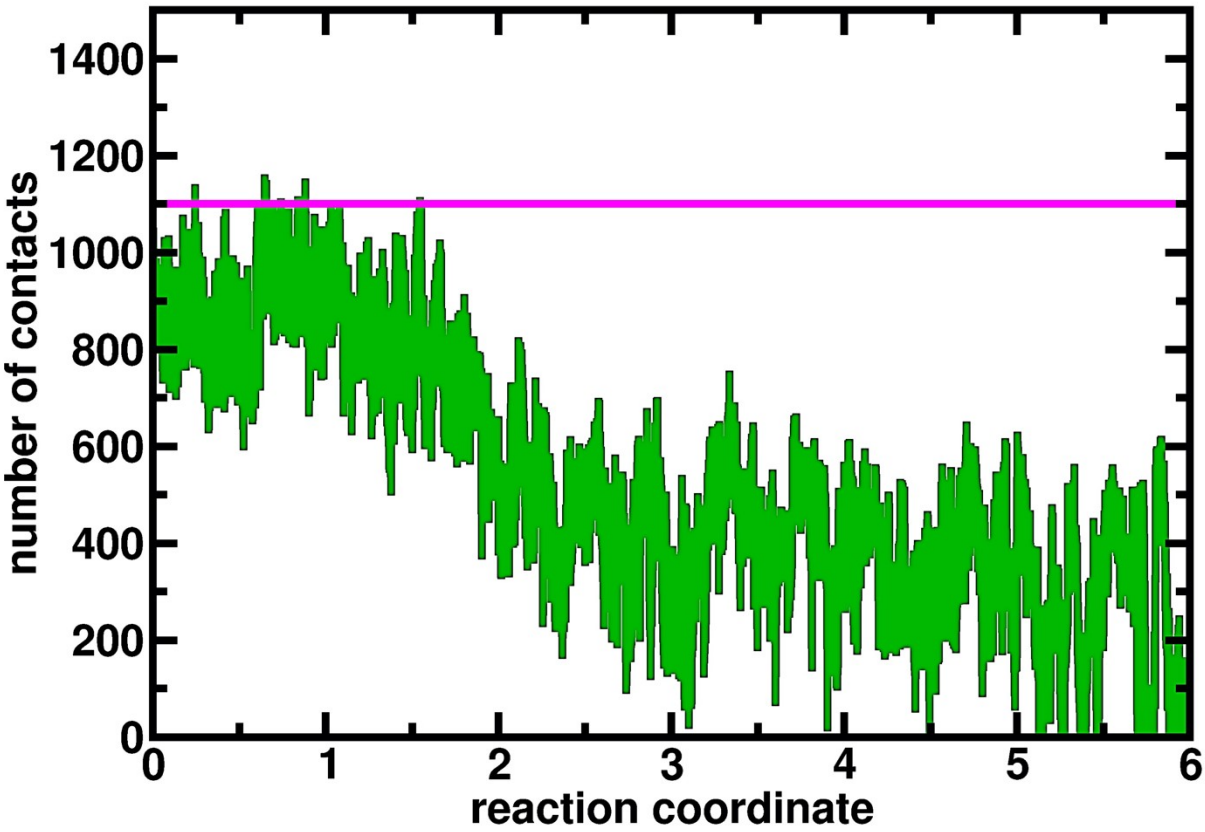

Figure S12: Variation in number of contacts between DRV and mPR as DRV was brought closer and closer to mPR along the reaction coordinate. The contact in the final model structure is indicated by solid magenta line.

Table S3: List of different regions in the HIVPR monomer and their constituent residues

Sl. No.	Region name	Residues in the region	Description
1	N-ter	1-4, 8	N-terminal
2	loop	5-7, 9	Loop
3	Ful	10-22	fulcrum
4	AS	23-30, 32, 76, 84	Active site
5	Bur	31, 33, 34, 77, 83, 85	Buried region
6	Elb	35-42	Flap elbow
7	Fl-ext	43-46, 55-58	Flap extension
8	Flap	47-54	Flap tip
9	UpC	59-62, 73-75	Upper cantilever
10	LoC	63-72	Lower cantilever
11	80s	78-82	80s loop
12	Hlx	86-94	helix
13	C-ter	95-99	C-terminal

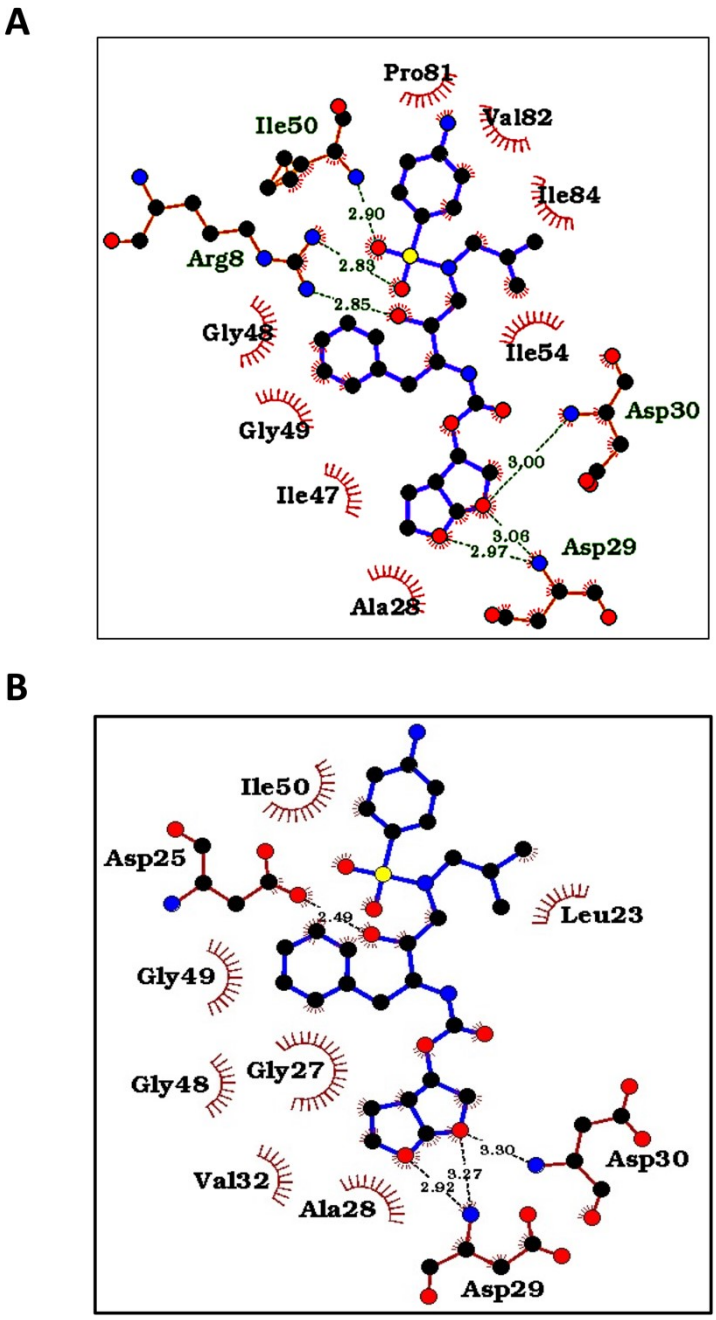

Figure S13: 2D interaction plot of DRV in (A) DRV-mPR complex, (B) crystal structure of DRV bound to dimeric HIVPR (interactions with second monomer are not shown for better comparison). The H-bond interactions between DRV and protein residues are represented by green dashed lines along with H-bond distance. Protease residues involved in H-bond interactions are shown in ball and stick representation. Other protein residues that are involved in nonpolar interactions with the ligand subsites are indicated as red spikes.